Applied and Computational Mathematics
2022; 11(5): 150-159
http://www.sciencepublishinggroup.com/j/acm
doi: 10.11648/j.acm.20221105.15
ISSN: 2328-5605 (Print); ISSN: 2328-5613 (Online)

Numerical Investigation of Unsteady Hydromagnetic Stokes Free-Convective Fluid Flow Past an Infinite Vertical Porous Plate with Variable Suction in a Rotating System

Mayaka Augustine Ayanga*, Mathew Ngugi Kinyanjui, Jeconia Okelo Abonyo, Johana Kibet Sigey

Department of Pure and Applied Mathematics, Jomo Kenyatta University of Agriculture and Technology, Nairobi, Kenya

Email address:

ayangaaugustine@gmail.com (Mayaka Augustine Ayanga), mathewkiny@jkuat.ac.ke (Mathew Ngugi Kinyanjui), masenooj@gmail.com (Jeconia Okelo Abonyo)

*Corresponding author

To cite this article:

Mayaka Augustine Ayanga, Mathew Ngugi Kinyanjui, Jeconia Okelo Abonyo, Johana Kibet Sigey. Numerical Investigation of Unsteady Hydromagnetic Stokes Free-Convective Fluid Flow Past an Infinite Vertical Porous Plate with Variable Suction in a Rotating System. *Applied and Computational Mathematics*. Vol. 11, No. 5, 2022, pp. 150-159. doi: 10.11648/j.acm.20221105.15

Received: August 30, 2022; **Accepted**: October 12, 2022; **Published**: October 24, 2022

Abstract: In this paper, Stokes first problem for an unsteady hydromagnetic free convective flow of a viscous incompressible fluid past an infinite vertical porous plate subjected to a variable suction in a rotating system has been studied. The specific equations governing the flow are nondimensionalized to obtain the dimensionless forms of the governing equations. The resulting dimensionless governing partial differential equations are solved numerically by the finite difference method based on the forward-time central-space scheme. The resulting numerical schemes are simulated in MATLAB software to obtain the profiles of the flow variables such as velocity, temperature, species concentration and magnetic induction. The main findings of this study are that an increase in the joule heating parameter results in a uniform increase in the velocity and temperature profiles near the plate but remain constantly distributed away from the plate. This observation implies that the flow is influenced substantially by the strength of joule heating near the plate and in the bulk of the fluid. The results are useful in industrial water treatment systems which rely on physical forces to aid in the removal of pollutants. Moreover, the results are applicable in the separation of isotopes contained in a mixture of very light molecular-weight gases such as hydrogen and helium and medium molecular-weight gases like nitrogen and air.

Keywords: Forward-Time-Central-Space, Hydromagnetic-Flow, Rotating-System, Stokes-Problem, Vertical-Porous-Plate, Variable-Suction

1. Introduction

The production of sheeting materials, such as polymer and metal sheet, arises in various industrial manufacturing processes. The quality of the final product depends on the rates of heat and mass transfer on the surface of the sheet. Therefore, the cooling rate of the plate and mass transfer rate should be effectively controlled so as to achieve the desired quality of the final product. Mass transfer plays an important role in many industrial processes such as the removal of pollutants from plant discharges streams by absorptions, the stripping of gases from waste water and diffusion of gases in nuclear power reactors.

In recent years, considerable attention has been focused in the study of heat and mass transfer in MHD flow due to its application in engineering devices (such as MHD power generators, MHD flow meters, MHD pumps, Hall accelerators and heat exchangers) and in industrial processes (such as metallurgy and material processing). Liquid metals are utilized in technological casting and cooling loops of nuclear reactors. The first research study on MHD flow was done by M. Faraday [1], who performed an experiment on the behavior of current in a circuit placed in an unsteady magnetic field. There are various theoretical studies in modeling the fluid flow past an infinite vertical porous plate. For example, Kinyanjui *et al.* studied heat and mass transfer in unsteady free convection flow with radiation absorption past an impulsively started infinite vertical porous plate

subjected to a strong magnetic field [2]. The model equations were solved by the finite difference method. The study analyzed the effects of various parameters on the velocity, temperature and concentration profiles, as well as skin friction and the rates of heat and mass transfer. The results revealed that cooling (or heating) of the plate by free convection currents has no effect on the rate of convection heat transfer at the surface of the plate. Also, an increase in the Schmidt number leads to a decrease in the rate of convection mass transfer at the surface of the plate.

Narahari *et al.* studied unsteady two-dimensional MHD free convection flow of a radiative fluid past an infinite vertical plate with constant heat and mass flux in the presence of thermal radiation and uniform magnetic field [3]. The model equations were solved analytically by the method of Laplace transform. The results obtained from the study revealed that the fluid velocity increases with an increase in the radiation parameter and decreases with an increase in the Hartmann number. This study neglected the effects of inertia on the boundary layer flow.

Murthy *et al.* studied Stokes first problem for the unsteady MHD natural convective flow past an infinite vertical porous plate with thermal radiation, Hall current, heat and mass transfer in presence of transverse magnetic field of uniform strength [4]. The model equations were solved both numerically by the finite element method and analytically by the perturbation technique. The results revealed that Hall current accelerates flow in the boundary layer region but decelerates the primary fluid velocity in the free-stream region. Further, thermal radiation accelerates both the primary and secondary velocities. Hall current and thermal radiation reduce the primary skin- friction but increase the secondary skin-friction. Moreover, the rate of heat transfer decreases with an increase in thermal radiation parameter.

Subbanna *et al.* studied unsteady MHD free convective flow of Newtonian fluid past an infinite vertical porous plate with time-dependent permeability and oscillatory suction in the presence of a uniform transverse magnetic field [5]. The model equations were solved semi-analytically by the perturbation method. The results revealed that Hartmann number, Prandtl number, and heat source parameter retard the flow while Grashof number and permeability parameter accelerate the flow. Also, the Schmidt number, suction velocity, and chemical reaction parameter reduce the species concentration. Further, the Grashof number, permeability parameter and suction velocity increase the shear stress at the plate while Hartmann number, Prandtl number, Schmidt number, chemical reaction parameter, and heat source parameter reduce the shear stress at the plate.

Finally, theoretical studies in modeling the MHD fluid flow in different flow configurations have also drawn the attention of many authors [6-15].

From the above previous modeling studies on fluid flow past an infinite vertical porous plate, it is noted that variable magnetic field, magnetic induction, joule heating, viscous dissipation, and rotating system have received little attention. The identified research gaps prevent the direct application of existing models to the sheeting industry. Therefore, the present study seeks to generalize the results of Krishna *et al.* [14] to include the effects of variable magnetic field, magnetic induction, joule heating, viscous dissipation, chemical reaction, heat source, Soret and Dufour effects for the case of a nonelastic fluid. The study results are essential in the sheeting industry and in the design of engineering devices which operate on the principles of MHD flow.

The rest of the paper is organized as follows: section II presents the model description and mathematical analysis, section III presents the numerical technique used to solve the corresponding model, section IV presents the results of the present study, and section V presents the conclusions drawn from the present study.

2. Mathematical Modeling

In this study, the unsteady MHD Stokes free convection flow of a viscous incompressible fluid past an infinite vertical porous plate subjected to variable suction is considered, as shown in Figure 1. A Cartesian coordinate system (x, y, z) is chosen such that x-axis is along the plate in the vertically upward direction, y-axis is normal to the plate and z-$axis is along the width of the plate (i.e., perpendicular to the xy-plane). The plate is infinite in extent in both x *and* z *directions, so the domain under consideration is* $-\infty < x < \infty$, $0 \le y < \infty$ *and* $-\infty < z < \infty$.

The plate and the fluid rotate as a rigid body with a constant angular velocity Ω *about the y-axis. A strong magnetic field* $\tilde{H}$ *of variable strength* H *is applied along the y-axis. At time* $t \le 0$, *the plate and the fluid are assumed to have the same uniform temperature* T_∞ *and the strength of the imposed magnetic field is* H_0. *At time* $t > 0$, *the plate starts moving impulsively along the positive x-axis with a uniform velocity* $U_0 > 0$ *and its temperature is instantaneously lowered or raised to* T_{wall}, *which is maintained constant thereafter. The species concentration at the plate is* C_{wall} *while that at the free-stream is* C_∞.

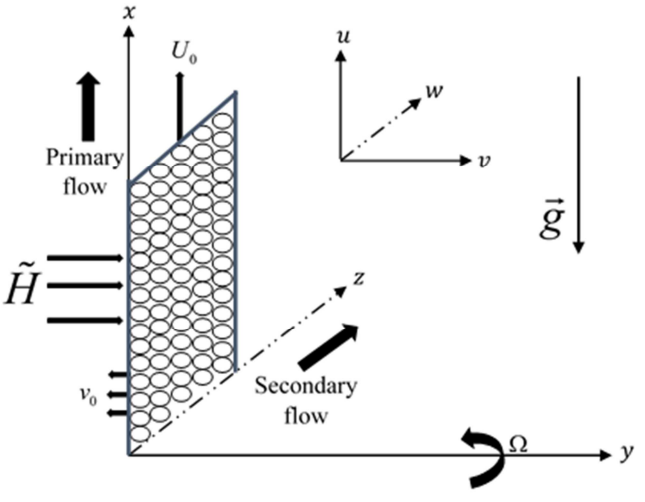

Figure 1. *Geometry of the research problem.*

Since the applied magnetic field is strong, the Hall current significantly affects the flow. The effect of Hall current gives rise to a force in a direction perpendicular to the xy-plane (i.e., in the z-direction), which induces a cross flow in that direction and hence the flow becomes three-dimensional. Since the plate is infinite in extent in both x and z directions and the flow is unsteady, the flow variables in this study are functions of y and t only. Since the applied magnetic field is of variable strength, its magnitude (H) is also a function of y and t.

2.1. Governing Equations

The general equations governing the flow problem in this study are as follows:

$$\frac{\partial \rho}{\partial t}+\vec{\nabla}\cdot\left(\rho\vec{V}\right)=0. \tag{1}$$

$$\rho\left[\frac{\partial \vec{V}}{\partial t}+\vec{V}\cdot\left(\vec{\nabla}\vec{V}\right)+2\Omega\times\vec{V}\right]=-\vec{\nabla}p-\frac{\mu}{\kappa}\vec{V}+\vec{\nabla}\cdot\left(\mu\vec{\nabla}\vec{V}\right)-\rho\vec{g}+\mathrm{J}\times\mathrm{B} \tag{2}$$

$$\left(\rho Cp\right)\left[\frac{\partial T}{\partial t}+\vec{V}\cdot\left(\vec{\nabla}T\right)\right]=\vec{\nabla}\cdot\left(k\vec{\nabla}T\right)+\Psi-\frac{\partial q_r}{\partial y}+\frac{\mathrm{J}\cdot\mathrm{J}}{\sigma}+Q_0\left(T-T_\infty\right)+\frac{\rho D_\mathrm{m}K_\mathrm{T}}{C_\mathrm{S}}\frac{\partial^2 C}{\partial y^2} \tag{3}$$

$$\frac{\partial C}{\partial t}+\vec{V}\cdot\left(\vec{\nabla}C\right)=\vec{\nabla}\cdot\left(D_\mathrm{m}\vec{\nabla}C\right)-K_\mathrm{r}\left(C-C_\infty\right)+\frac{D_\mathrm{m}K_\mathrm{T}}{T_\mathrm{m}}\frac{\partial^2 T}{\partial y^2} \tag{4}$$

$$\mathrm{J}+\frac{m}{|\mathrm{B}|}\left(\mathrm{J}\times\mathrm{B}\right)=\sigma\left(\mathrm{E}+\vec{V}\times\mathrm{B}\right) \tag{5}$$

$$\frac{\partial \mathrm{B}}{\partial t}=\vec{\nabla}\times\left(\vec{V}\times\mathrm{B}\right)-\vec{\nabla}\times\left(D_\mathrm{B}\vec{\nabla}\times\mathrm{B}\right) \tag{6}$$

In this study, all the fluid properties are assumed to be constants, there is no-slip condition at the plate, the fluid is electrically conducting and the plate is non-conducting. Using Boussinesq and boundary layer approximations, the governing equations of continuity, momentum, energy, concentration, and magnetic induction are given by

$$\frac{\partial v}{\partial y}=0 \quad \Rightarrow \quad v=-v_0\left(1+\epsilon e^{nt}\right) \tag{7}$$

$$\rho\left[\frac{\partial u}{\partial t}+v\frac{\partial u}{\partial y}+2\Omega w\right]=-\frac{\mu}{\kappa}u+\mu\frac{\partial^2 u}{\partial y^2}+\rho g\beta_T\left(T-T_\infty\right)+\rho g\beta_C\left(C-C_\infty\right)-\frac{\sigma\mu_\mathrm{e}^2H_0^2\sqrt{H_x^2+H_0^2}\left[\sqrt{H_x^2+H_0^2}u+mH_0w\right]}{\left[H_x^2+H_0^2\left(1+m^2\right)\right]} \tag{8}$$

$$\rho\left[\frac{\partial w}{\partial t}+v\frac{\partial w}{\partial y}-2\Omega u\right]=-\frac{\mu}{\kappa}w+\mu\frac{\partial^2 w}{\partial y^2}+\frac{\sigma\mu_\mathrm{e}^2H_0^2\sqrt{H_x^2+H_0^2}\left[mH_0u-\sqrt{H_x^2+H_0^2}w\right]}{\left[H_x^2+H_0^2\left(1+m^2\right)\right]} \tag{9}$$

$$\left(\rho Cp\right)\left[\frac{\partial T}{\partial t}+v\frac{\partial T}{\partial y}\right]=k\left(1+\frac{16\sigma_0T_\infty^3}{3k_0k}\right)\frac{\partial^2 T}{\partial y^2}+\mu\left[\left(\frac{\partial u}{\partial y}\right)^2+\left(\frac{\partial w}{\partial y}\right)^2\right]+Q_0\left(T-T_\infty\right)+\frac{\sigma\mu_\mathrm{e}^2H_0^2\left(H_x^2+H_0^2\right)}{\left[H_x^2+H_0^2\left(1+m^2\right)\right]}\left(u^2+w^2\right)+\frac{\rho D_\mathrm{m}K_\mathrm{T}}{C_\mathrm{S}}\frac{\partial^2 C}{\partial y^2} \tag{10}$$

$$\frac{\partial C}{\partial t}+v\frac{\partial C}{\partial y}=D_\mathrm{m}\frac{\partial^2 C}{\partial y^2}-K_\mathrm{r}\left(C-C_\infty\right)+\frac{D_\mathrm{m}K_\mathrm{T}}{T_\mathrm{m}}\frac{\partial^2 T}{\partial y^2} \tag{11}$$

$$\frac{\partial H_x}{\partial t}=H_0\frac{\partial u}{\partial y}+D_\mathrm{B}\frac{\partial^2 H_x}{\partial y^2} \tag{12}$$

2.2. Boundary and Initial Conditions

Equations (7)--(12) are solved subject to the following initial and boundary conditions, for $y\geq 0$ and $t\geq 0$.

$$u = 0, w = 0, T = T_\infty, C = C_\infty, H_x = 0 \quad \text{at } t = 0 \tag{13}$$

$$u = U_0, w = 0, T = T_{\text{wall}}, C = C_{\text{wall}}, H_x = H_0 \text{ at } y = 0 \tag{14}$$

$$u = 0, w = 0, T = T_\infty, C = C_\infty, H_x = 0 \text{ as } y \to \infty \tag{15}$$

2.3. Non-dimensionalization

In this study, the characteristic length is taken as $\mu/(\rho U_0)$ and the characteristic velocity is taken as the velocity of the plate U_0. Therefore, the characteristic time is $\mu/(\rho U_0^2)$. To non-dimensionalize the specific governing equations (7)—(12) together with the initial and boundary conditions (13)—(15), the following dimensionless variables are introduced.

$$\bar{y} = \frac{y}{\mu/(\rho U_0)}, \bar{t} = \frac{t}{\mu/(\rho U_0^2)}, \bar{n} = \frac{n}{(\rho U_0^2)/\mu} \tag{16}$$

$$\bar{u} = \frac{u}{U_0}, \bar{v} = \frac{v}{U_0}, \bar{w} = \frac{w}{U_0}, \bar{v}_0 = \frac{v_0}{U_0} \tag{17}$$

$$\theta = \frac{T - T_\infty}{T_{\text{wall}} - T_\infty}, \phi = \frac{C - C_\infty}{C_{\text{wall}} - C_\infty}, h = \frac{H_x}{H_0} \tag{18}$$

Using the chain rule of differentiation, the dimensionless forms of the specific governing equations are obtained as:

$$\frac{\partial \bar{v}}{\partial \bar{y}} = 0 \quad \Rightarrow \quad \bar{v} = -\bar{v}_0\left(1 + \epsilon e^{\bar{n}\bar{t}}\right) \tag{19}$$

$$\frac{\partial \bar{u}}{\partial \bar{t}} + \bar{v}\frac{\partial \bar{u}}{\partial \bar{y}} + 2\mathrm{R_o}\bar{w} = -\frac{1}{\mathrm{K}}\bar{u} + \frac{\partial^2 \bar{u}}{\partial \bar{y}^2} + \mathrm{Gr_T}\theta + \mathrm{Gr_C}\phi - \mathrm{M}^2\frac{\sqrt{h^2+1}\left[\sqrt{h^2+1}\bar{u} + m\bar{w}\right]}{\left[h^2 + \left(1+m^2\right)\right]} \tag{20}$$

$$\frac{\partial \bar{w}}{\partial \bar{t}} + \bar{v}\frac{\partial \bar{w}}{\partial \bar{y}} - 2\mathrm{R_o}\bar{u} = -\frac{1}{\mathrm{K}}\bar{w} + \frac{\partial^2 \bar{w}}{\partial \bar{y}^2} + \mathrm{M}^2\frac{\sqrt{h^2+1}\left[m\bar{u} - \sqrt{h^2+1}\bar{w}\right]}{\left[h^2 + \left(1+m^2\right)\right]} \tag{21}$$

$$\frac{\partial \theta}{\partial \bar{t}} + \bar{v}\frac{\partial \theta}{\partial \bar{y}} = \frac{1}{\mathrm{Pr}}(1+\mathrm{N})\frac{\partial^2 \theta}{\partial \bar{y}^2} + \frac{\delta}{\mathrm{Pr}}\theta + \mathrm{Ec}\left[\left(\frac{\partial \bar{u}}{\partial \bar{y}}\right)^2 + \left(\frac{\partial \bar{w}}{\partial \bar{y}}\right)^2\right] + \mathrm{Du}\frac{\partial^2 \phi}{\partial \bar{y}^2} + \mathrm{R}\frac{\left(h^2+1\right)}{\left[h^2 + \left(1+m^2\right)\right]}\left(\bar{u}^2 + \bar{w}^2\right) \tag{22}$$

$$\frac{\partial \phi}{\partial \bar{t}} + \bar{v}\frac{\partial \phi}{\partial \bar{y}} = \frac{1}{\mathrm{Sc}}\frac{\partial^2 \phi}{\partial \bar{y}^2} - \gamma\phi + \mathrm{Sr}\frac{\partial^2 \theta}{\partial \bar{y}^2} \tag{23}$$

$$\frac{\partial h}{\partial \bar{t}} = \frac{\partial \bar{u}}{\partial \bar{y}} + \frac{1}{\mathrm{R_m}}\frac{\partial^2 h}{\partial \bar{y}^2} \tag{24}$$

subject to the following initial and boundary conditions

$$\bar{u}(\bar{y}, 0) = 0,\ \bar{w}(y, 0) = 0,\ \theta(\bar{y}, 0) = 0,\ \phi(\bar{y}, 0) = 0,\ h(\bar{y}, 0) = 0 \tag{25}$$

$$\bar{u}(0, \bar{t}) = 1,\ \bar{w}(0, \bar{t}) = 0,\ \theta(0, \bar{t}) = 1,\ \phi(0, \bar{t}) = 1,\ h(0, \bar{t}) = 1 \tag{26}$$

$$\bar{u}(\infty, \bar{t}) = 0,\ \bar{w}(\infty, \bar{t}) = 0,\ \theta(\infty, \bar{t}) = 0,\ \phi(\infty, \bar{t}) = 0,\ h(\infty, \bar{t}) = 0 \tag{27}$$

3. Numerical Procedure

The initial boundary value problem (IBVP) given by equations (10a) to (10f) is solved numerically using forward-time central-space (FTCS) scheme. The computational domain is confined by the $\bar{y}$ axis and $\bar{t}$ axis. The $\bar{y}$ -values range from 0 to $\bar{y}_{\max}$, where $\bar{y}_{\max}$ is a large finite value that approximates the conditions at infinity. The $\bar{t}$ -values range from 0 to $\bar{t}_{\max}$. The closed interval $[0, \bar{y}_{\max}]$ is divided into N_y sub-intervals of equal width $\Delta\bar{y}$. The $\bar{y}$ -values at the grid points are denoted by $\bar{y}_i$ for $i = 0,1,2,\cdots,N_y$. The closed interval $[0, \bar{t}_{\max}]$ is divided into N_t sub-intervals of equal width $\Delta\bar{t}$. The $\bar{t}$ -values at the grid points are denoted by $\bar{t}_j$ for $j = 0,1,2,\cdots,N_t$. The task is to approximate the values of the unknown functions $\bar{u}(\bar{y},\bar{t}), \bar{w}(\bar{y},\bar{t}), \theta(\bar{y},\bar{t}), \phi(\bar{y},\bar{t})$ and $h(\bar{y},\bar{t})$ at the grid points $(\bar{y}_i, \bar{t}_j)$ in the discretized domain, where $\bar{y}_i = i\Delta\bar{y}$ and $\bar{t}_j = j\Delta\bar{t}$. For instance, the discrete approximation of the primary velocity $\bar{u}(\bar{y},\bar{t})$ at the grid point $(\bar{y}_i, \bar{t}_j)$ is denoted by $\bar{u}_{i,j}$ or $\bar{u}(\bar{y}_i, \bar{t}_j)$. Similarly, the discrete approximation of the species concentration $\phi(\bar{y},\bar{t})$ at the grid point $(\bar{y}_i, \bar{t}_j)$ is denoted by $\phi_{i,j}$, etc. The nodes at $i = 0$ and $i = N_y$ define the boundaries of the computational domain while the time level $j = 0$ defines the initial conditions.

In the FTCS scheme, the derivatives with respect to time ($\bar{t}$) are approximated using forward difference scheme while the derivatives with respect to space variables ($\bar{y}$) are approximated using central difference scheme at the j^{th} time level. Thus, the discretized form of the dimensionless governing equations are given as:

$$\bar{v}_{i+1,j} - \bar{v}_{i-1,j} = 0 \quad \Rightarrow \quad \bar{v}_{i,j} = -\bar{v}_0\left(1 + \epsilon e^{\bar{n}\bar{t}_j}\right) \tag{28}$$

$$\bar{u}_{i,j+1} = \bar{u}_{i,j} + \Delta\bar{t}\left\{-\bar{v}_{i,j}\frac{\bar{u}_{i+1,j} - \bar{u}_{i-1,j}}{2\Delta\bar{y}} - 2\mathrm{R_o}\bar{w}_{i,j} - \frac{1}{\mathrm{K}}\bar{u}_{i,j} + \frac{\bar{u}_{i+1,j} - 2\bar{u}_{i,j} + \bar{u}_{i-1,j}}{\left(\Delta\bar{y}\right)^2} + \mathrm{Gr_T}\theta_{i,j} + \mathrm{Gr_C}\phi_{i,j} - \mathrm{M}^2\frac{\sqrt{h_{i,j}^2+1}\left[\sqrt{h_{i,j}^2+1}\bar{u}_{i,j} + m\bar{w}_{i,j}\right]}{\left[h_{i,j}^2 + \left(1+m^2\right)\right]}\right\} \tag{29}$$

$$\bar{w}_{i,j+1} = \bar{w}_{i,j} + \Delta\bar{t}\left\{-\bar{v}_{i,j}\frac{\bar{w}_{i+1,j} - \bar{w}_{i-1,j}}{2\Delta\bar{y}} + 2\mathrm{R_o}\bar{u}_{i,j} + \frac{\bar{w}_{i+1,j} - 2\bar{w}_{i,j} + \bar{w}_{i-1,j}}{\left(\Delta\bar{y}\right)^2} - \frac{1}{\mathrm{K}}\bar{w}_{i,j} + \mathrm{M}^2\frac{\sqrt{h_{i,j}^2+1}\left[m\bar{u}_{i,j} - \sqrt{h_{i,j}^2+1}\bar{w}_{i,j}\right]}{\left[h_{i,j}^2 + \left(1+m^2\right)\right]}\right\} \tag{30}$$

$$\theta_{i,j+1} = \theta_{i,j} + \Delta\bar{t}\left\{-\bar{v}_{i,j}\frac{\theta_{i+1,j} - \theta_{i-1,j}}{2\Delta\bar{y}} + \frac{1}{\mathrm{Pr}}(1+\mathrm{N})\frac{\theta_{i+1,j} - 2\theta_{i,j} + \theta_{i-1,j}}{\left(\Delta\bar{y}\right)^2} + \mathrm{Ec}\left[\left(\frac{\bar{u}_{i+1,j} - \bar{u}_{i-1,j}}{2\Delta\bar{y}}\right)^2 + \left(\frac{\bar{w}_{i+1,j} - \bar{w}_{i-1,j}}{2\Delta\bar{y}}\right)^2\right] + \mathrm{R}\frac{\left(h_{i,j}^2+1\right)}{\left[h_{i,j}^2 + \left(1+m^2\right)\right]}\left(\bar{u}_{i,j}^2 + \bar{w}_{i,j}^2\right) + \frac{\delta}{\mathrm{Pr}}\theta_{i,j} + \mathrm{Du}\frac{\phi_{i+1,j} - 2\phi_{i,j} + \phi_{i-1,j}}{\left(\Delta\bar{y}\right)^2}\right\} \tag{31}$$

$$\phi_{i,j+1} = \phi_{i,j} + \Delta\bar{t}\left\{-\bar{v}_{i,j}\frac{\phi_{i+1,j} - \phi_{i-1,j}}{2\Delta\bar{y}} + \frac{1}{\mathrm{Sc}}\frac{\phi_{i+1,j} - 2\phi_{i,j} + \phi_{i-1,j}}{\left(\Delta\bar{y}\right)^2} - \gamma\phi_{i,j} + \mathrm{Sr}\frac{\theta_{i+1,j} - 2\theta_{i,j} + \theta_{i-1,j}}{\left(\Delta\bar{y}\right)^2}\right\} \tag{32}$$

$$h_{i,j+1} = h_{i,j} + \Delta\bar{t}\left\{\frac{\bar{u}_{i+1,j} - \bar{u}_{i-1,j}}{2\Delta\bar{y}} + \frac{1}{\mathrm{R_m}}\frac{h_{i+1,j} - 2h_{i,j} + h_{i-1,j}}{\left(\Delta\bar{y}\right)^2}\right\} \tag{33}$$

The corresponding finite difference approximations of the initial and boundary conditions are given by:

$$\bar{u}_{i,0} = 0, \bar{w}_{i,0} = 0, \theta_{i,0} = 0, \phi_{i,0} = 0, h_{i,0} = 0 \tag{34}$$

$$\bar{u}_{0,j} = 1, \bar{w}_{0,j} = 0, \theta_{0,j} = 1, \phi_{0,j} = 1, h_{0,j} = 1 \tag{35}$$

$$\bar{u}_{N_y,j} = 0, \bar{w}_{N_y,j} = 0, \theta_{N_y,j} = 0, \phi_{N_y,j} = 0, h_{N_y,j} = 0 \tag{36}$$

In the first iteration, the solutions for the unknown functions $\bar{u}, \bar{w}, \theta, \phi$ and h are determined at time level $j = 0$, where the

initial approximations are obtained from the initial conditions given by equation (34). The iteration is repeated for $j = 1, 2, \cdots, N_t$. The numerical computations have been performed with the aid of MATLAB software for $N_y = 20, N_t = 150, \bar{y}_{\min} = 0, \bar{y}_{\max} = 1$ and $\Delta\bar{y} = (\bar{y}_{\max} - \bar{y}_{\min}) / N_y$. The time step in this study is taken as $\Delta\bar{t} = (\Delta\bar{y})^2 / 8$, which satisfies the stability condition. The simulation results are presented graphically and discussed in the next section.

4. Results and Discussion

The flow variables in this study are the primary velocity, secondary velocity, temperature, species concentration and magnetic induction. The various flow parameters that have been varied include the magnetic parameter (M^2) , Hall parameter (m) , Eckert number (Ec) , Joule heating parameter (R) , radiation parameter (N) , chemical reaction parameter (γ) , heat source parameter (δ) , rotation parameter (R_o) , magnetic Reynolds number (R_m) , Dufour number (Du) , Soret number (Sr) , Schmidt number (Sc) , Prandtl number (Pr) , thermal Grashof number (Gr_T) , mass Grashof number (Gr_C) , and suction parameter $(\bar{v}_0)$, at time $t = 0.1887$. These parameters are input into a computer program where each parameter is varied at a time. The Prandtl number $Pr = 0.71$ corresponds to air. The Grashof number $Gr > 0$ corresponds to cooling of the plate by free convection currents. In this study, the magnetic parameter $M^2 \geq 5$ signifies a strong magnetic field.

4.1. Effects of Varying Mass Grashof Number

Figure 2 shows that an increase in mass Grashof number leads to an increase in both the primary and secondary velocity profiles. The mass Grash of number defines the ratio of the species buoyancy force to the viscous force. As expected, the fluid velocity increases due to increase in the species buoyancy force. The mass Grashof number defines the ratio of the species buoyancy force to the viscous hydrodynamic force. As expected, the fluid velocity increases and the peak value is more distinctive due to increase in the species buoyancy force.

4.2. Effects of Varying Thermal Grash of Number

Figure 3 shows that an increase in thermal Grashof number leads to an increase in both the primary and secondary velocity profiles. Thermal Grashof number represents the effects of free convection currents and a positive value physically corresponds to heating of the fluid (or cooling of the plate). Velocity of the fluid increases because the fluid flow is assisted by the free convection currents. As expected, increase in the velocity profiles is due to the enhancement of thermal buoyancy force. The observed increase in secondary velocity profiles with increase in thermal Grashof number is as a result of emergence of secondary circulation currents due to the presence of the temperature gradient. The thermal Grashof number represents the effect of the thermal buoyancy force relative to the viscous hydrodynamic force. The flow is accelerated due to the enhancement of the buoyancy force corresponding to the increase in thermal Grashof number. The positive values of thermal Grashof number correspond to cooling of the plate by free convection. Hence, heat is conducted away from the vertical plate into the fluid, which increases the temperature and thereby enhancing the buoyancy force. The observed increase in velocity profiles is due to the increase in buoyancy force with increasing Grash of number.

4.3. Effects of Varying Rotation Parameter

Figure 4 shows that an increase in rotation parameter leads to a decrease in the primary velocity profiles but an increase in the secondary velocity profiles. This means rotation can be used to control the velocity profiles in a rotating system.

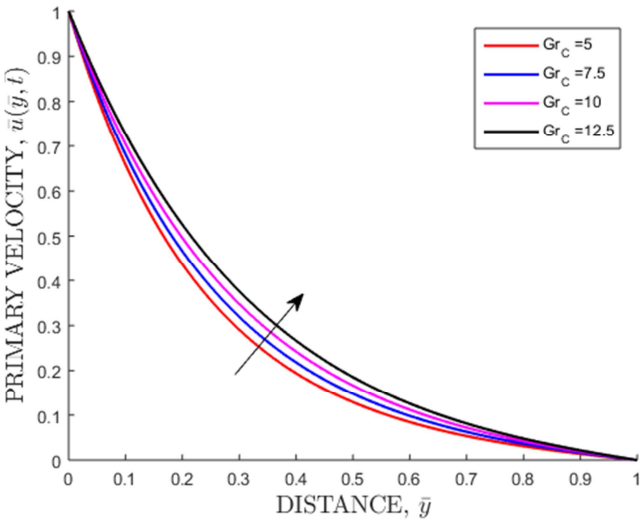

(a) Primary Velocity Profiles

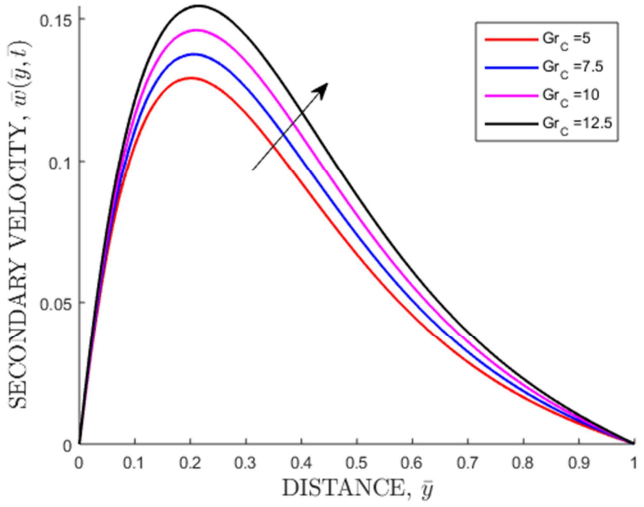

(b) Secondary Velocity Profiles

Figure 2. *Velocity profiles for different values of mass Grashof number.*

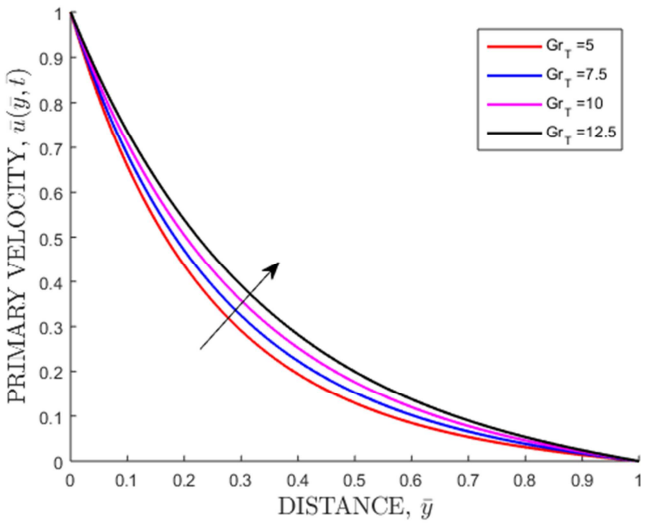

(a) Primary Velocity Profiles

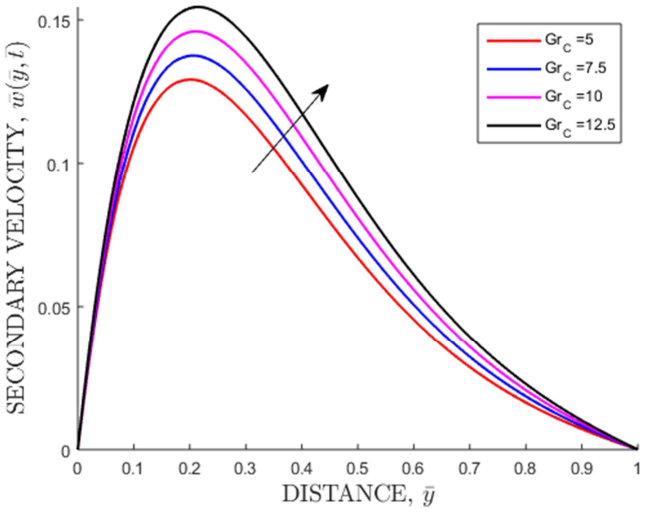

(b) Secondary Velocity Profiles

Figure 3. *Velocity profiles for different values of thermal Grashof number.*

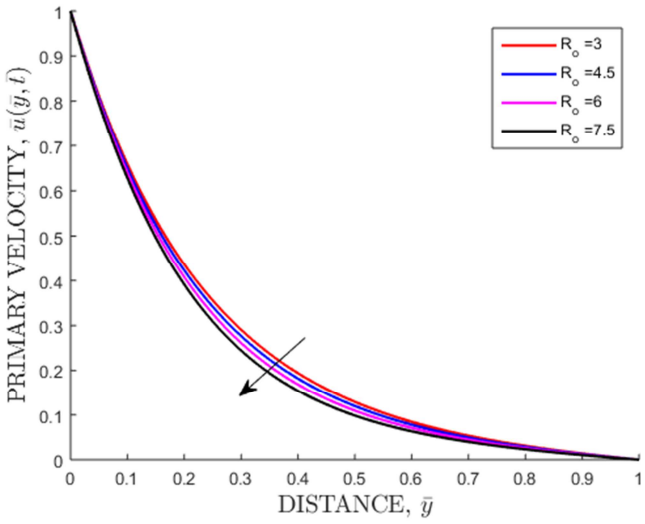

(a) Primary Velocity Profiles

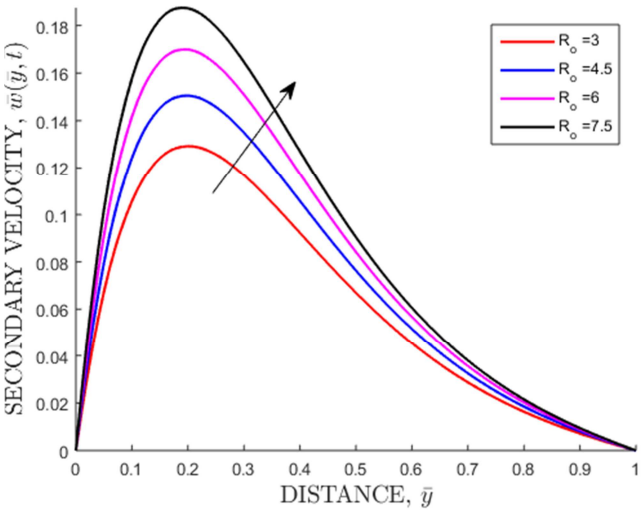

(b) Secondary Velocity Profiles

Figure 4. *Velocity profiles for different values of magnetic parameter (R_0).*

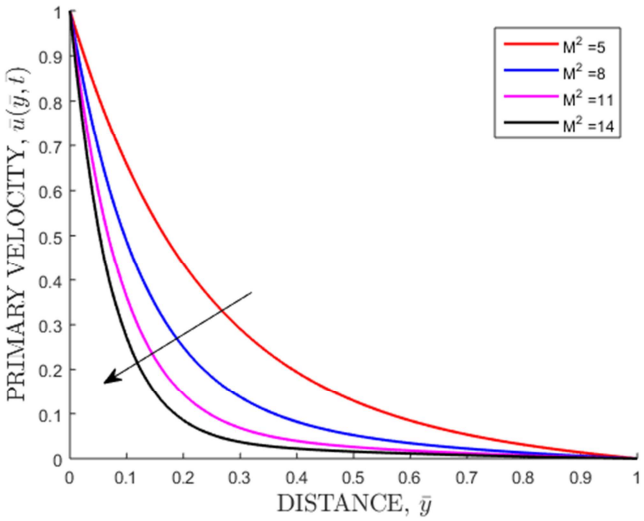

(a) Primary Velocity Profiles

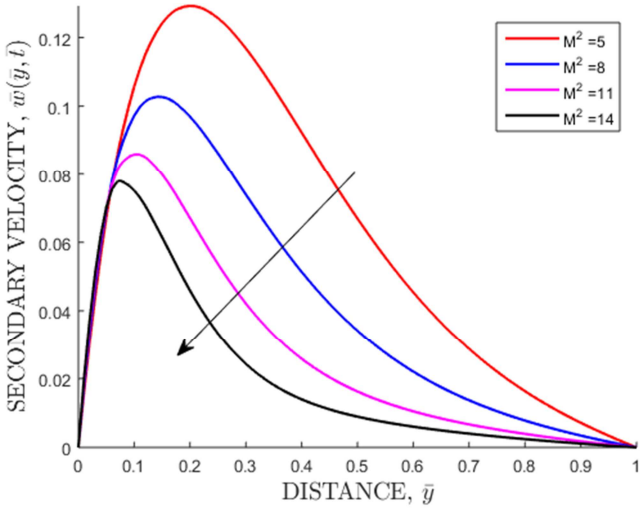

(b) Secondary Velocity Profiles

Figure 5. *Velocity profiles for different values of magnetic parameter (M^2).*

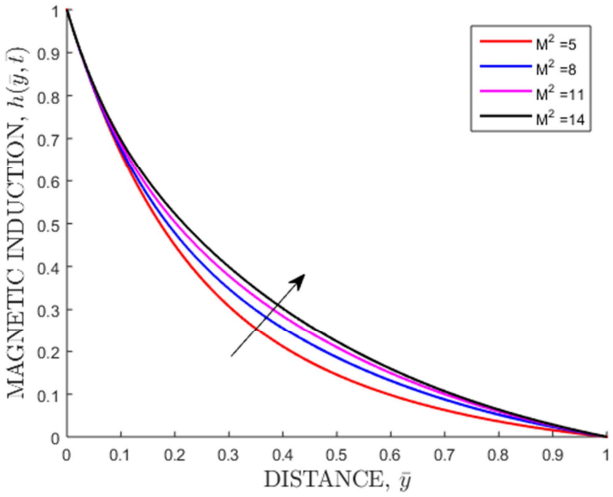

Figure 6. *Induction profiles for different values of magnetic parameter (M^2).*

4.4. Effects of Varying Magnetic Parameter

Figure 5 shows that an increase in magnetic parameter leads to a decrease in both the primary and secondary velocity profiles. This is because the application of a transverse magnetic field to an electrically conducting fluid gives rise to a resistive force called the Lorentz force, which has the tendency to slow down the motion of the fluid in the velocity boundary layer. Figure 6 shows that an increase in magnetic parameter leads to a increase in magnetic induction profiles. Further, the magnetic damping force increases with increasing magnetic parameter, causing a decrease in the velocity profiles. Magnetic field can, therefore, be employed to control the velocity boundary layer characteristics of a fluid. The Lorentz force acts against the flow since the magnetic field is applied in the normal direction, hence retarding the motion.

4.5. Effects of Varying Hall Parameter

Figure 7 shows that an increase in Hall parameter leads to an increase in both the primary and secondary velocity profiles. This is because increase in Hall parameter leads to decrease in the conductivity of the fluid, reducing the magnetic damping force.

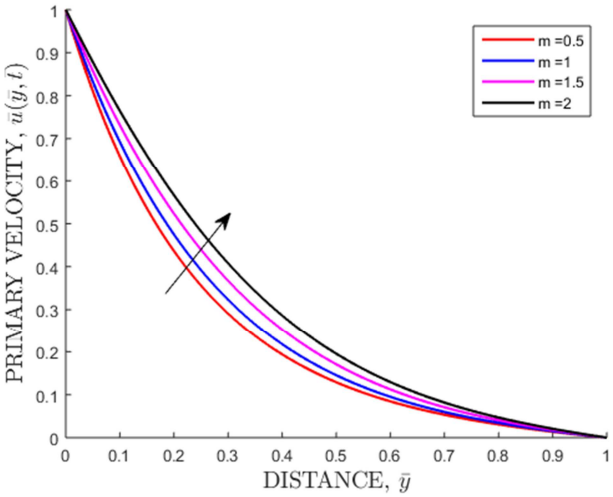

(a) Primary Velocity Profiles

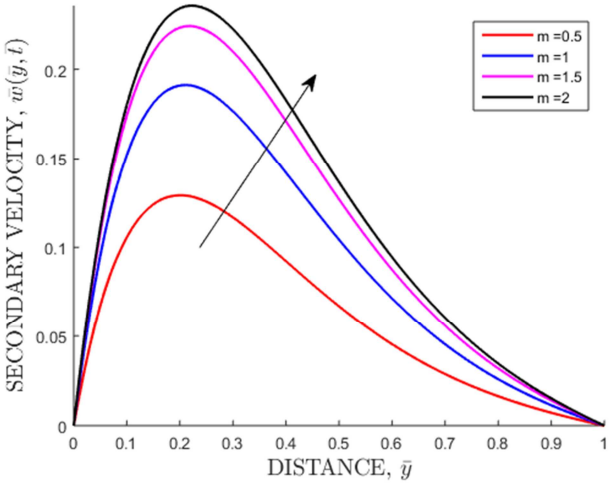

(b) Secondary Velocity Profiles

Figure 7. *Velocity profiles for different values of Hall parameter (m).*

4.6. Effects of Varying Suction Parameter

Figure 8 shows that an increase in sunction parameter leads to a decrease in both the primary and secondary velocity profiles.

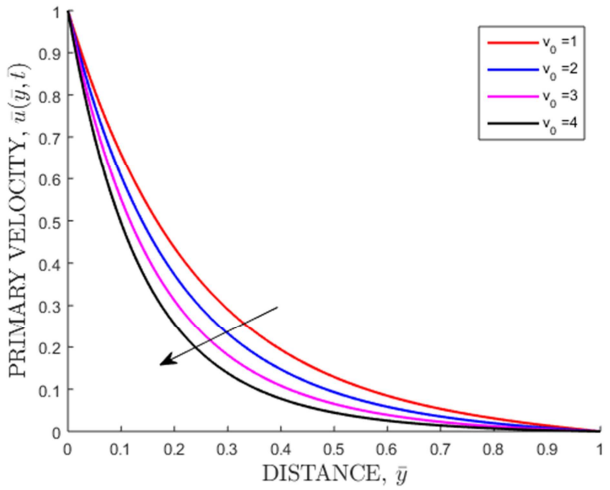

(a) Primary Velocity Profiles

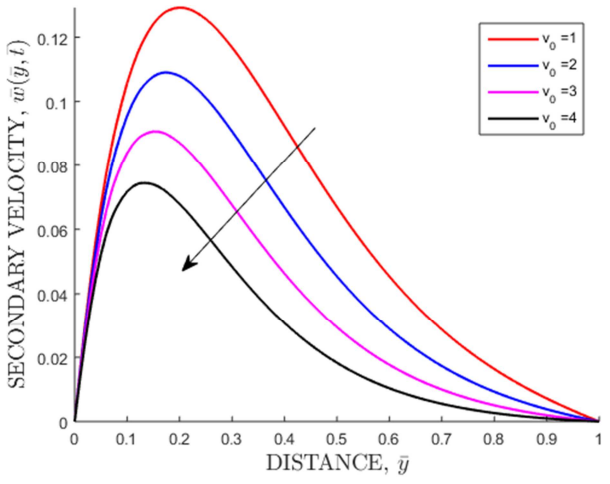

(b) Secondary Velocity Profiles

Figure 8. *Velocity profiles for different values of suction parameter v_0.*

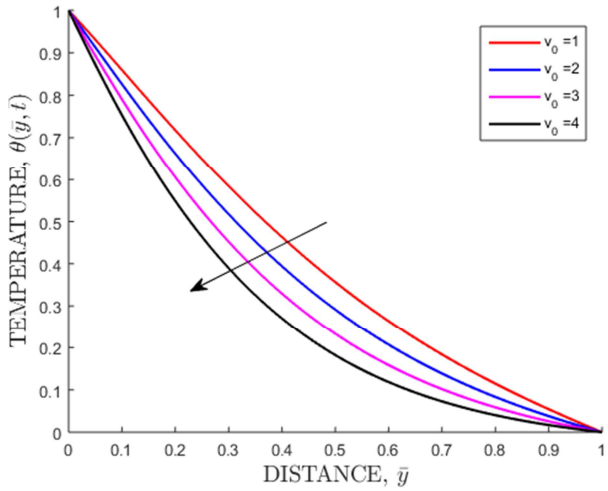

Figure 9. *Temperature profiles for different values of suction parameter* v_0.

Figure 9 shows that an increase in sunction parameter leads to a decrease in both the temperature profiles.

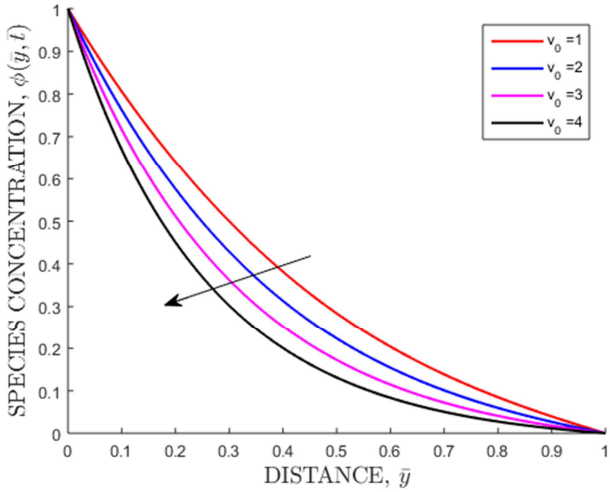

Figure 10. *Concentration profiles for different values of suction parameter* v_0.

Figure 10 shows that an increase in suction parameter leads to a decrease in both the concentration profiles. Suction decreases the velocity of the fluid thus decreasing the rate at which the species are carried away from the boundary layer region, and hence the observed decrease in the species concentration. Thus velocity, temperature and concentration boundary layers can be controlled by varying the rate of suction. The results mean that introducing suction can be used to destabilize the velocity, thermal and concentration boundary layers. This indicates the usual fact that suction destabilizes the growth of the boundary layer.

5. Conclusion

The FTCS schemes used in the computations in this study are stable and consistent. The effects of various flow parameters on unsteady hydromagnetic Stokes free convection flow of a viscous, incompressible and electrically conducting fluid past an impulsively started infinite vertical porous plate subjected to variable suction in a rotating system with heat and mass transfer in the presence of a strong, non-uniform magnetic field normal to the plate have been investigated by varying the parameters. The important findings in this study are:

i. Velocity of the fluid can be controlled by introducing a porous medium in a rotating system.
ii. Introducing injection/suction can be used to control the boundary layer growth, the shear stresses and rates of heat transfer and mass transfer.
iii. Rotation can be used to control the magnitude of shear stresses and the boundary layer formation over a stretching sheet.
iv. Introducing porous media in a flow domain can be used to control the velocity, concentration and temperature of the fluid.
v. The Hall effects can be utilized in controlling the fluid's velocity, concentration, temperature and sheer stress and the rates of heat and mass transfer respectively.

Acknowledgements

The authors would like to thank the academic and technical support of Jomo Kenyatta University of Agriculture and Technology (JKUAT) especially Kisii CBD campus for providing the necessary learning resources to facilitate the successful completion of this research project. The library, computer and other facilities of the University have been indispensable. Augustine Mayaka thanks the chairman, members of staff in the department of pure and applied mathematics and his colleagues for their support and making his stay in the department pleasant and memorable.

References

[1] M. Faraday, "Electricity researches in electricity," 1st Series Philosophical Transactions of the Royal Society, pp. 125–162, 1831.

[2] M. Kinyanjui, J. Kwanza, and S. Uppal, "Magnetohydrodynamic free convection heat and mass transfer of a heat generating fluid past an impulsively started infinite vertical porous plate with hall current and radiation absorption," Energy conversion and management, vol. 42, no. 8, pp. 917–931, 2001.

[3] M. Narahari, S. Tippa, and R. Pendyala, "Unsteady magnetohydrodynamic free convection flow of a radiative fluid past an infinite vertical plate with constant heat and mass flux," in Applied Mechanics and Materials, vol. 465. Trans Tech Publ, 2014, pp. 149–154.

[4] M. R. Murthy, R. S. Raju, and J. A. Rao, "Heat and mass transfer effects on mhd natural convective flow past an infinite vertical porous plate with thermal radiation and hall current," Procedia Engineering, vol. 127, pp. 1330–1337, 2015.

[5] K. Subbanna, S. G. Mohiddin, and R. B. Vijaya, "Combined effects on mhd flow of newtonian fluid past infinite vertical porous plate," in AIP Conference Proceedings, vol. 1953, no. 1. AIP Publishing LLC, 2018, p. 140099.

[6] F. O. Ochieng, "Hydromagnetic jeffery-hamel unsteady flow of a dissipative non-newtonian fluid with nonlinear viscosity," Ph.D. dissertation, JKUAT-PAUSTI, 2018.

[7] B. Parent, M. N. Shneider, and S. O. Macheret, "Generalized ohms law and potential equation in computational weakly-ionized plasma dynamics," Journal of Computational Physics, vol. 230, no. 4, pp. 1439–1453, 2011.

[8] M. Kinyanjui, M. Emmah, J. Marigi, and K. Kwanza, "Hydromagnetic turbulent flow of a rotating system past a semiinfinite vertical plate with hall current.," International Journal of Heat and Mass transfer, vol. 79, pp. 97–119, 2012.

[9] M. Moorthy and K. Senthilvadivu, "Soret and dufour effects on natural convection flow past a vertical surface in a porous medium with variable viscosity," Journal of Applied Mathematics, vol. 2012, 2012.

[10] K. Giterere, "Magnetohydrodynamic flow in porous media over a stretching surface in a rotating system with heat and mass transfer," Ph.D. dissertation, 2013.

[11] A. Maguna and N. Mutua, "Hall current effects on free convection flow and mass transfer past semi-infinite vertical flat plate," Int. Jnl. of Mathematics and Statistics Studies, vol. 1, no. 4, pp. 1–22, 2013.

[12] H. Zaman, A. Sohail et al., "Stokes first problem for an unsteady mhd third-grade fluid in a non-porous half space with hall currents," Open Journal of Applied Sciences, vol. 2014, 2014.

[13] N. Marneni, S. Tippa, and R. Pendyala, "Ramp temperature and dufour effects on transient mhd natural convection flow past an infinite vertical plate in a porous medium," The European Physical Journal Plus, vol. 130, no. 12, p. 251, 2015.

[14] M. V. Krishna, M. G. Reddy, and A. Chamkha, "Heat and mass transfer on mhd rotating flow of second grade fluid past an infinite vertical plate embedded in uniform porous medium with hall effects," in Applied Mathematics and Scientific Computing. Springer, 2019, pp. 417–427.

[15] J. Pattnaik, G. Dash, and S. Singh, "Diffusion-thermo effect with hall current on unsteady hydromagnetic flow past an infinite vertical porous plate," Alexandria Engineering Journal, vol. 56, no. 1, pp. 13–25, 2017.